Journal of Power Sources 196 (2011) 10369–10379

Contents lists available at ScienceDirect

Journal of Power Sources

journal homepage: www.elsevier.com/locate/jpowsour

Optimal decentralized charging control algorithm for electrified vehicles connected to smart grid

Changsun Ahn*, Chiao-Ting Li, Huei Peng

Department of Mechanical Engineering, The University of Michigan, G041 Auto Lab. 1231 Beal Av., Ann Arbor, MI 48109, USA

ARTICLE INFO

Article history:
Received 9 June 2011
Received in revised form 27 June 2011
Accepted 27 June 2011
Available online 2 July 2011

Keywords:
Charging control
Decentralized control
Electrified vehicle
Grid-to-vehicle (G2V)
Valley-filling
Frequency regulation

ABSTRACT

Electrified vehicles (EV) and renewable power sources are two important technologies for sustainable ground transportation. If left unmitigated, the additional electric load could over-burden the electric grid. Meanwhile, a challenge for integrating renewable power sources into the grid lies in the fact their intermittency requires more regulation services which makes them expensive to deploy. Fortunately, EVs are controllable loads and the charging process can be interrupted. This flexibility makes it possible to manipulate EV charging to reduce the additional electric load and accommodate the intermittency of renewable power sources. To illustrate this potential, a two-level optimal charging algorithm is designed, which achieves both load shifting and frequency regulation. Load shifting can be realized through coordination of power generation and vehicle charging while reducing power generation cost and carbon dioxide emissions. To ensure practicality, a decentralized charging algorithm for load shifting is formulated by emulating the charging pattern identified through linear programming optimization solutions. The frequency regulation is also designed based on frequency droop that can be implemented in a decentralized way. The two control objectives can be integrated because they are functionally separated by time scale. Simulation results are presented to demonstrate the performance of the proposed decentralized algorithm.

1. Introduction

Electrified vehicles and renewable power sources are actively pursued as clean energy technologies. However, the former can increase the electric grid load during charging, which could stress generation and transmission systems. The latter are intermittent in nature and can bring challenging regulation problems when they are integrated with the grid.

In the past, increased electric demand has mostly been met by building extra centralized power plants. The electric infrastructure was designed to meet the peak demands which only occur a few hundred hours each year in the US [1]. The peak power costs more because it uses more expensive fuels and have shorter running hours than the base powers do. If the peak demand can be redistributed to less congested hours, such as during early morning, the additional plants for the peak power might not need to be built. This is the so-called load shifting strategy. Electrified vehicles are controllable loads and can even be power sources (i.e., they can return energy back to the grid) under extraneous situations [2]. Most EVs are plugged-in for long hours during the night, i.e., exactly during the valley hours of traditional electric grid. Therefore, we can manipulate the charging pattern of EVs to achieve load shifting or valley filling.

Regulation is a short time scale ancillary service usually conducted by fast-reacting power sources. The power sources for regulation respond to a system-operator's request to track the minute-by-minute fluctuations in system load and to respond to unintended fluctuations in generator output [3]. They are expensive to operate due to the stand-by characteristics of the service and their responsiveness. When wind and solar power sources are introduced, they require a higher level of regulation services, resulting in increased regulation cost. One of the benefits of EVs is their response time. Due to this characteristic, EVs can replace some of the regulation service units.

Different approaches to realizing these two potential benefits (load shifting and regulation) have been presented in the literature. The cases in which vehicles provide power to the grid, V2G (vehicle-to-grid), have been studied [4,5]. A number of studies [6–9] focused on the regulation capability of EV batteries and have shown that V2G may be beneficial to the grid operations, sometimes at the expense of lower battery charging completion. Furthermore, these approaches are based on a short time horizon and have not explored long-term behaviors such as valley-filling or load shifting. Even though the benefit of EV load shifting has been studied in many

* Corresponding author. Tel.: +1 734 846 4288; fax: +1 734 647 9732.
E-mail address: sunahn@umich.edu (C. Ahn).

0378-7753/$ – see front matter © 2011 Elsevier B.V. All rights reserved.
doi:10.1016/j.jpowsour.2011.06.093

Nomenclature

Acronyms

EV	electrified vehicle
V2G	vehicle to grid
AC	alternating current
SOC	state of charge
LP	linear programming

Symbols

P	power
τ_2, τ_3	time constants of power plants
k_I, k_p	integral and proportional gains of a controller
ω	frequency
H	normalized inertial constant
D	normalized damping constant
P_{EV}	charging power of EV
$P_{EV\max}$	the maximum charging power of EV
P_{nonEV}	non-EV power demand
$P_{EV,SFT}$	EV charging power that contributes demand shifting
$P_{EV,REG}$	EV charging power that contributes frequency regulation
$P_{EV,REG}$	EV charging power that contributes frequency regulation
N_{EV}	the number of EVs connected to the grid
$C(n)$	battery capacity of EV #n

papers [1,10–12], few papers have presented how to realize EV load shifting. Recently, some papers [13,14] have begun to design non-centralized strategies for valley-filling. Ma et al. [13] and Callaway and Hiskens [14] showed that a demand dependent pricing scheme drives a unique Nash equilibrium that results in valley-filling. This algorithm works in a decentralized way but requires that all vehicles have access to information of other vehicles and the grid power generation, so the developed algorithm requires a lot of communications. Furthermore, it does not provide a closed form of the charging algorithm. In theory, a centralized controller can collect full information of all EVs and all power plants, utilizing future power demand and control all vehicles/plants simultaneously for optimal performance. Such an approach, however, requires extensive bi-directional communication and heavy computations and thus is not desirable. A decentralized charging controller requires smaller amount of information to be collected and exchanged. Most of the existing algorithms of load shifting are centralized and thus require more infrastructure for implementation. Furthermore, most of them are based on thermal load [15,16] or air-conditioning load [17] control not on EV load control. Besides, most papers [6–9,13,14] on the V2G framework presented only one control objective, regulation or load shifting, but not both.

In our design, the decentralized and distributed charging controllers receive a simple command from the centralized grid controller and they only have access to the information from the local vehicle (e.g., battery state of charge) and the local grid (e.g., AC frequency). Designing such decentralized charging control algorithms that achieve near-optimal performance (compared to a centralized controller) is the goal and the main contribution of this paper. In this paper, we present a decentralized charging control algorithm that minimizes electricity generation cost and carbon dioxide emissions. The algorithm also regulates charging power to mitigate uncertainties due to renewable power sources. The controller is developed with two separate time scales: a load shifting algorithm on a long time scale and a frequency regulation algorithm on a short time scale. Effects of the two algorithms are separated due to time scale and the algorithms can be easily combined without compromising their performance. The remainder of the paper is organized as follows: the problem is defined in Section 2; the design of the load shifting algorithm is explained in Section 3; the frequency regulation algorithm is presented in Section 4; the integration and overall structure and performance of the controller are presented in Sections 5 and 6; and finally a conclusion is given in Section 7.

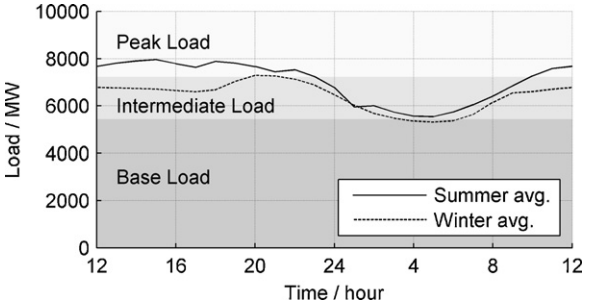

Fig. 1. Average non-EV power demand profile of the DTE service area.

2. Problem statement

2.1. Grid and demand

In this paper, the area supported by DTE Energy in Michigan is used to determine the size the power generation and load [18]. The electric power demand in this area varies between 5000 MW and 8000 MW, with the summer load higher than the winter load due to air-conditioning. Peak electric demand occurs around 2 pm in the summer and 7 pm in the winter. The lowest demand occurs around 4 am. The hourly power demand profiles for typical summer and winter days are shown in Fig. 1, where the load below 5500 MW is defined as the base load, the load between 5500 and 7200 MW is defined as intermediate load, and above 7200 MW is defined as peak load. The summer profile will be used for this paper. The same design process of course can be used for the winter load.

2.2. Generation units and frequency dynamics

All electric grid systems have multiple types of generation sources. The first type is base load sources that have the cheapest operating cost. The second type is load following units which are used to make up the difference between the demand and the base load power. The third type of power sources are regulation units and are used for frequency regulation. The characteristics of the three types of power sources are summarized in Table 1. The base load power plants are assumed to follow a planned profile and be the same as the forecasted power demand. The load following units and regulation units are modeled as first order systems controlled by an integral controller and a proportional controller, respectively [19], as shown in Eqs. (1) and (2)

$$P_1 = P_{planned}, \quad P_2 = \frac{1}{1+\tau_2 s}P_{follow}, \quad P_3 = \frac{1}{1+\tau_3 s}P_{reg}, \tag{1}$$

where P_1, P_2 and P_3 are the power output from the three types of power source. τ_2 and τ_3 are the time constants for the second and third type of power plants. The power generation strategy to regulate the frequency is simplified as follows:

$$P_{follow} = -k_I \int \Delta\omega \; dt, \quad P_{reg} = -k_p \Delta\omega, \tag{2}$$

where k_I and k_p are control gains designed to stabilized the system and $\Delta\omega$ is a deviation from the desired frequency value, 60 Hz in

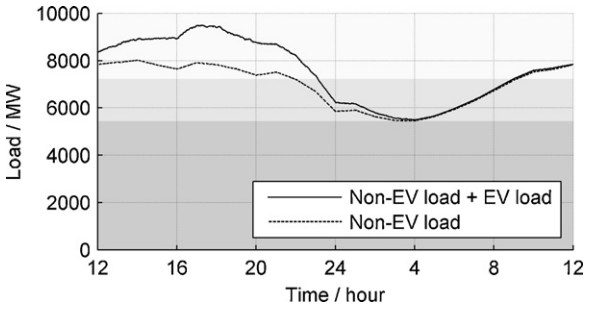

Fig. 2. Power demand profile when the charging of the 2 M EVs are unmitigated (charging at the maximum power level immediately after plug in).

US. The frequency of the grid is modeled as first-order rotational dynamics, as follows:

$$H\dot{\omega} + D\omega = P_m - P_e, \tag{3}$$

where H is the inertial constant in normalized (per) unit, D is a damping coefficient in per unit, $P_m = P_1 + P_2 + P_3$ is the total power input to the grid and P_e is the total electric power demand.

2.3. Electrified vehicles and commuting patterns

The number of EVs is assumed to be two million, which is about 25% of the registered passenger vehicles in Michigan. The commuting pattern of the vehicle owners is assumed as follows: the owners leave home for work at 7:20 am with 2 h of standard deviation; they return home around 4:30 pm with 4.3 h of standard deviation; the battery state of charge (SOC) when plugged-in is also described by a normal distribution with a mean of 0.5 and a standard deviation of 0.1; the vehicles are charged only during the night (not at work). The mean and standard deviation of the commuting patterns are based on the traffic count data from Interstate Highway 5 [20]. The battery capacity is assumed to be 16 kWh, all vehicle are assumed to be charged by level-I chargers at 110 V/15 A, and the allowed SOC range is assumed to be 0.3–0.85.

If we simulate a scenario where every EV starts charging at maximum power at the moment they are plugged in, the charging power will add to the grid load, as shown in Fig. 2. The additional EV demand increases the peak demand and causes the peak load plants to operate, which have significantly higher electricity generation cost.

2.4. Renewable power source and uncertainties

In this study, electric power from a wind farm is assumed to be part of the grid. The National Renewable Energy Laboratory (NREL) provides forecasted and observed wind power datasets for many places in the US [21]. For the algorithm verification purposes, we examined forecasted and observed wind power profiles from the database. An example is shown in Fig. 3. We assumed 10% penetration rate of renewable power sources in nominal capacity. The forecasted profile will be included in the base load generation and the observed profiles gives uncertainties, the effect of which is mitigated by regulation services.

Table 1
Characteristics of the power plants categorized by service types.

Services	Base load	Load following	Regulation
Control	Feed forward	Integral	Proportional
Time scale	Hour–day	10–100 min	ms–min

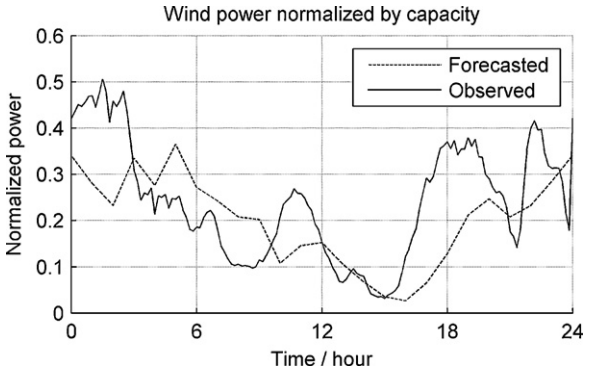

Fig. 3. Example wind power profile from the NREL database (June 22nd 2006, site # 3939).

2.5. Generation cost and CO_2 emissions

A service provider typically manages many power plants that can be categorized into base load plants, intermediate load plants, and peak load plants. Nuclear and coal power plants are usually used for the base load, combined cycle power plants for the intermediate load, and gas turbines for the peak load. In this cost structure, we take into account only the energy cost so that the cost of regulation services is not included. The generation cost curves are based on economic dispatch rules for the service providers. The instantaneous cost curve for the target grid is derived using the method reported in [22], as shown in Fig. 4(a). The carbon dioxide emission curve is achieved by using carbon dioxide emission tables for different fuel types [23] and plant types [24,25], as shown in Fig. 4(b). To minimize production cost and carbon dioxide emission, we combined these two curves using a carbon tax concept [26]. The combined cost curve with a carbon tax ($12 per tonne of CO_2) is shown in Fig. 5.

2.6. Objectives and constraints

The first objective is to develop a decentralized algorithm that charges the EV's battery as much as possible while minimizing the generating cost and carbon dioxide emissions of power plants. The secondary objective is to reduce the dependency of conventional regulation plants. To accomplish the objectives, the EV loads have to be shifted to the valley hours to minimize the operation of the peak

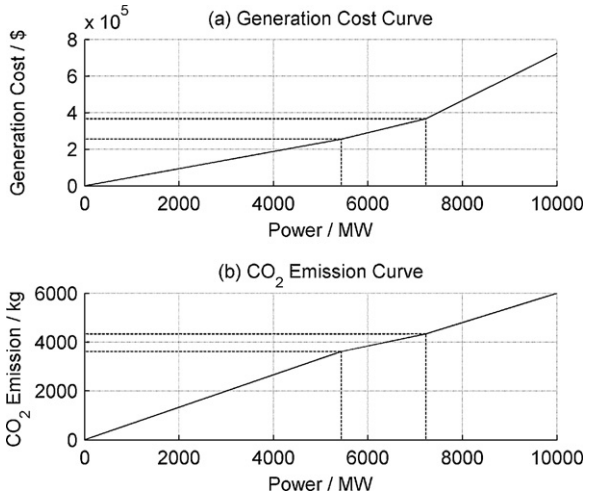

Fig. 4. (a) Power generation cost curve and (b) CO_2 emission curve.

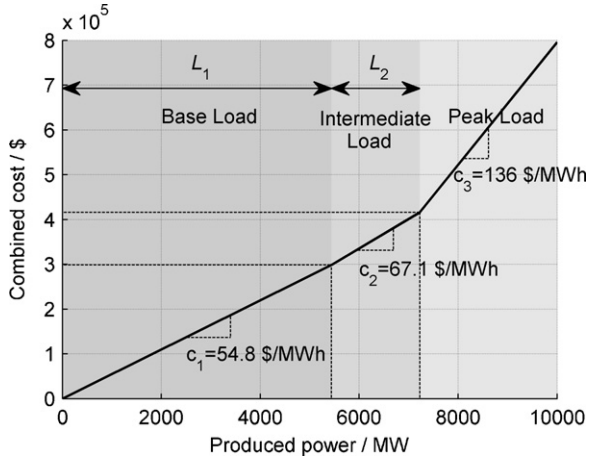

Fig. 5. Combined cost curve, $C(P(t))$, (Generation cost + CO_2 emission), the carbon tax of \$12/tCO_2 is used.

load plants, and the EV charging algorithm should have a frequency regulation capability.

2.7. Approaches

The overall grid system and the charging controller are shown in Fig. 6. To achieve the design objectives, we developed a sub-optimal control algorithm that balances among multiple objectives: minimization of the power generation cost and carbon dioxide emissions. The problem was first solved as a linear programming (LP) problem. Subsequently, a near-optimal decentralized control algorithm is formulated by emulating the optimal charging pattern obtained from the LP solution. The optimal decentralized control algorithm uses a few pieces of information to compute the charging power: the forecasted total power demand of the grid, estimated plug off time, and the battery SOC of the local vehicle.

For frequency regulation, we utilize a frequency droop based power control algorithm in order not to degrade the performance of the load shifting algorithm while keeping the overall control structure in a decentralized manner.

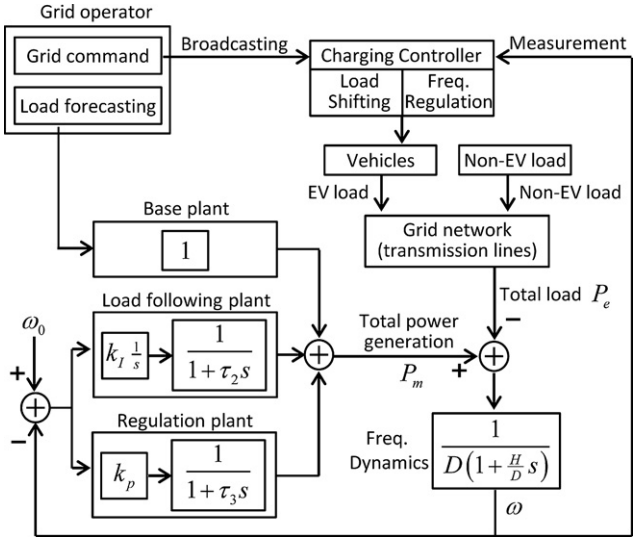

Fig. 6. The electricity grid model with the proposed charging controller.

3. Load shifting

The design process begins by solving the LP optimal control problem where all information is available and a central controller determines the charging power of each EV and the power generation of each plant. The solution of the control problem provides important information: the optimal control pattern for each EV. A decentralized charging control algorithm can then be obtained by emulating the behavior of the LP solution. The remaining contents of this chapter include: formulation of the optimal control problem; solution to the problem using LP technique; analysis of the optimal control patterns; and derivation of the decentralized control algorithm.

3.1. Formulation of the optimal control problem

The cost function to be minimized is the electricity generation cost and total carbon dioxide emissions. Given the cost curve, $C(P(t))$, shown in Fig. 5, the optimal control problem is defined as follows:

$$\min_{P_{EV}(t,n)} \sum_{t=0}^{T} C(P(t)), \tag{4}$$

where

$$P(t) = \sum_{n=1}^{N} P_{EV}(t,n) + P_{nonEV}(t), \tag{5}$$

$$C(P(t)) = c_1 \cdot \min(P(t), L_1) + c_2 \cdot \min(\max(P(t) - L_1, 0), L_2) + c_3 \cdot \max(P(t) - L_1 - L_2, 0), \tag{6}$$

$P_{nonEV}(t)$ is the non-EV electric load and $P_{EV}(t,n)$ is the control variable for $t = 0, 1, 2, \ldots, T$, $n = 1, 2, 3, \ldots, N$. L_1 and L_2 are the power levels when the cost curve gets bended and defined in Fig. 5. The constraints for the optimization problem include

$$\sum_{t=0}^{T} P_{EV}(t,n) \cdot \Delta t = B(n), \tag{7}$$

$$0 \le P_{EV}(t,n) \le P_{EV\,\mathrm{lim}}(t,n), \tag{8}$$

where $B(n)$ is the total energy to charge the battery of car # n as much as it can during the plug-in time, for $n = 1, 2, 3, \ldots, N$, so that $B(n)$ is given in this optimization formulation. $P_{EV\mathrm{lim}}(t)$ is the charging power limit of the battery, determined as follows:

$$P_{EV\,\mathrm{lim}}(t,n) = \begin{cases} P_{EV\,\max}, & \text{when the vehicle } n \text{ is on-line} \\ 0, & \text{when the vehicle } n \text{ is off-line} \end{cases}. \tag{9}$$

Eq. (5) represents the total power demand consisting of the non-EV load and the EV charging load; Eq. (7) requires that all EVs must be charged as much as unmitigated, which prevents EVs from sacrificing charging completion for reducing power generation. Eq. (8) reflects the fact that the charging power of each EV is limited by the maximum current, and no vehicle-to-grid power flow is allowed. Eq. (9) requires that EVs are charged only when they are plugged in.

When the combined cost curve is not linear then typically a nonlinear optimization problem with a large number of control variables needs to be solved, which requires tremendous computing power. Fortunately, the cost curve is piece-wise linear and has increasing slope. Therefore, we can use linear programming (LP) to solve the problem by adding more control variables and constraints.

3.2. Solution through linear programming

The formulated optimization problem can be solved by modifying the cost function, as follows:

$$\min_{P_{EV}(t,n)} \sum_{t=0}^{T} (c_1 \cdot q_1(t) + c_2 \cdot q_2(t) + c_3 \cdot q_3(t)), \tag{10}$$

where $0 < c_1 < c_2 < c_3$ are defined in Fig. 5. The constraints consist of linear constraints and conditional constraints. The linear constraints are

$$q_1(t) + q_2(t) + q_3(t) = \sum_{n=1}^{N} P_{EV}(t, n) + P_{nonEV}(t), \tag{11}$$

$$\sum_{t=0}^{T} P_{EV}(t, n) = B(n), \tag{12}$$

$$0 \le P_{EV}(t, n) \le P_{EV\,\mathrm{lim}}(t, n), \tag{13}$$

$$0 \le q_1(t) \le L_1, \quad 0 \le q_2(t) \le L_2, \quad 0 \le q_3(t). \tag{14}$$

And the conditional constraints are

$$\begin{aligned}
&\text{if } P(t) < L_1, && \begin{cases} q_1(t) = P(t), \\ q_2(t) = 0, \qquad q_3(t) = 0, \end{cases} \\
&\text{if } L_1 \le P(t) < L_2, && \begin{cases} q_1(t) = L_1, \\ q_2(t) = P(t) - L_1, \quad q_3(t) = 0, \end{cases} \\
&\text{if } P(t) \ge L_1 + L_2, && \begin{cases} q_1(t) = L_1, \qquad\qquad q_2(t) = L_2, \\ q_3(t) = P(t) - L_1 - L_2, \end{cases}
\end{aligned} \tag{15}$$

where $q_1(t)$, $q_2(t)$, and $q_3(t)$ vary only in the linear ranges of the piece-wise linear cost curve. The introduction of new variables transforms the nonlinear cost function to a linear cost function and in the meantime adds the conditional constraints. However, these conditional constraints are not active (the optimal solution does not exist in the hyper-plane defined by the conditional constraints), as proved in Appendix. Therefore, we can ignore the conditional constraints and the problem can be solved using a standard linear programming technique.

3.3. Optimal results and analysis

The parameters of the optimization problem are as follows: $T = 24$ with 1 h step, $N = 100$ (the two million EVs are grouped into 100 sets). The plug-in time, plug-off time, and the initial SOCs are randomly generated based on the commute pattern, and their values are assumed to be known to the centralized controller. The problem is solved using the LP solver in MATLAB (linprog) and the results are plotted in Fig. 7. In the optimal solution, the additional load due to EV charging fills the valley of the demand profile during the night so that the peak power plant does not need to operate. If we compare the demand profile of Fig. 7(b) with that of Fig. 2, we can see that the EV charging demand is shifted to early morning hours. Fig. 7(c) shows examples of optimal charging patterns. The EVs begin to charge as soon as the valley period begins, which is defined as the time when the base demand is below the peak load line, where we do not need to turn on the peak load plants. The EVs also finish their charging when the valley period ends. The charging power depends on the battery SOC: the EV with a lower SOC uses higher charging power. The charging power also depends on the amount of available grid power.

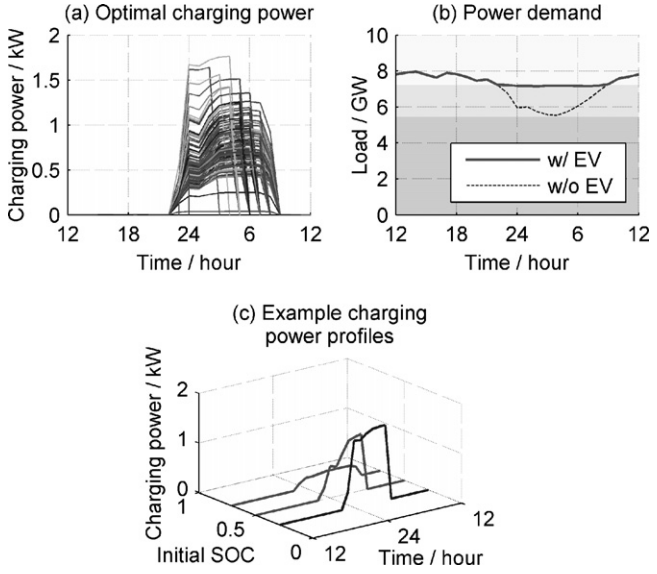

Fig. 7. Optimal results obtained from LP: (a) the charging pattern of EVs; (b) the resulting electric power demand; and (c) three examples of charging patterns for different SOC levels.

3.4. Development of the decentralized control algorithm

To analyze the charging pattern, the EVs are grouped by the plug-off time, as shown in Fig. 8. The charging power of EVs that have the same plug-off time shows linear dependency to SOC, and the sensitivity changes over time. As a result, the charging power can be expressed as:

$$P_{EV,SFT}(t, n) = K(t, n) \cdot (SOC_{\max} - SOC(t, n)), \tag{16}$$

where $SOC_{\max}$ is the maximum allowable SOC that is 0.85 in this problem. The gradient $K(t, n)$ is computed from the LP solutions and plotted in Fig. 9. The gradient increases as the time to plug-off decreases, and as the time to valley-end decreases. Also, the amount of available cheap power affects $K(t, n)$.

Another way to derive $P_{EV,SFT}(t, n)$ is based on the observation that charging power is highly related to the amount of available cheap power, which is defined as $L_1 + L_2 - P_{nonEV}(t)$. For perfect valley-filling, the following equation must hold:

$$\sum_{n=1}^{N} P_{EV,SFT}(t, n) = L_1 + L_2 - P_{nonEV}(t). \tag{17}$$

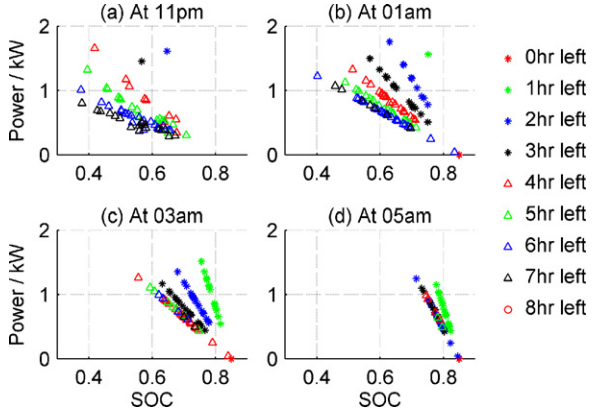

Fig. 8. Optimal charging power from the LP solutions was found to be proportional to "SOC deficit".

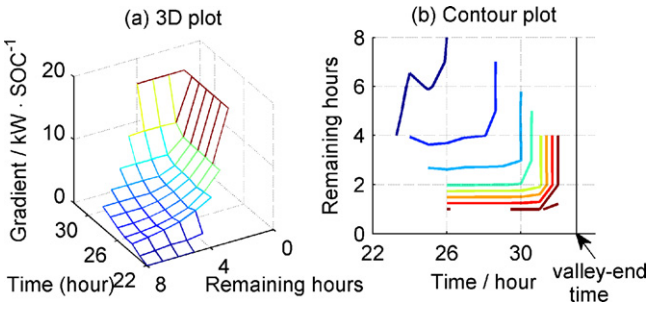

Fig. 9. Charging gradient function, $K(t, n)$, computed using the optimal solutions.

Then, the average charging power per vehicle at time t is calculated as follows:

$$\bar{P}_{EV,SFT}(t) = \frac{\sum_{n=1}^{N} P_{EV,SFT}(t,n)}{N_{EV}(t)} = \frac{L_1 + L_2 - P_{nonEV}(t)}{N_{EV}(t)}, \tag{18}$$

where $N_{EV}(t)$ is the number of EVs that are plugged in. In this stage, $P_{nonEV}(t)$ and $N_{EV}(t)$ are assumed known for all t. Using this average charging power, we propose another charging algorithm:

$$P_{EV,SFT}(t,n) = R(t,n) \cdot \bar{P}_{EV,SFT}(t), \tag{19}$$

where $R(t, n)$ is the charging gain. Because the EV's battery should be fully charged by the end of valley hours or the plug-off time, the following equation must hold:

$$SOC_{\max} - SOC(t,n) = \frac{1}{C(n)} \int_t^{T_n} P_{EV}(\tau,n) \cdot d\tau$$

$$= \frac{1}{C(n)} \int_t^{T_n} R(\tau,n) \cdot \bar{P}_{EV,SFT}(\tau) \cdot d\tau, \tag{20}$$

where $T_n = \min(t_{plug\text{-}off,n}, t_{valley\text{-}end})$ and $C(n)$ is the battery capacity of EV #n. Because we do not know future $R(\tau, n)$, it is assumed to be time invariant and we have:

$$R(t,n) = \frac{C(n) \cdot (SOC_{\max} - SOC(t,n))}{\int_t^{T_{end}} \bar{P}_{EV,SFT}(\tau) \cdot d\tau}. \tag{21}$$

This calculated $R(t, n)$ is assumed to be constant until $\bar{P}_{EV,SFT}(t)$ and $SOC(t, n)$ are updated. Plug (21) into (19), we have

$$P_{EV,SFT}(t,n) = \frac{C(n) \cdot \bar{P}_{EV,SFT}(t)}{\int_t^{T_n} \bar{P}_{EV,SFT}(\tau) \cdot d\tau} (SOC_{\max} - SOC(t,n)), \tag{22}$$

which is the equation of the decentralized charging algorithm. We should point out that $K(t, n)$ in Eq. (16) can be calculated by comparing Eqs. (16) and (22):

$$K(t,n) = \frac{C(n) \cdot \bar{P}_{EV,SFT}(t)}{\int_t^{T_n} \bar{P}_{EV,SFT}(\tau) \cdot d\tau}, \tag{23}$$

where $\bar{P}_{EV,SFT}(t) = L_1 + L_2 - P_{nonEV}(t)/N_{EV}(t)$.

The gradient $K(t, n)$ in Eq. (23) should be verified by comparing against the LP solution. To see the robustness of this gradient function, two different power profiles are used. Fig. 10 compares the gradient values from the optimization results and from Eq. (23). An imagined double valley profile is used as a challenging case. Even though the gradient function was derived using a single valley profile, it matches well with LP results calculated from the double valley profile, which shows the robustness of the gradient function. The parameters of the controller should be determined by two separate players. $C(n)$ is determined by the EV designer and L_1 L_2 and $N_{EV}(t)$ should be by the grid operator in consideration of the generation cost structure.

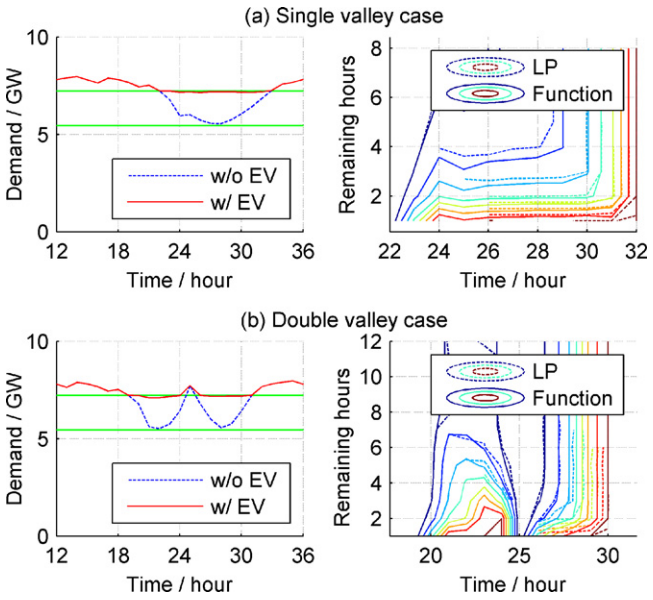

Fig. 10. Verification of the robustness of the gradient function $K(t, n)$.

The control algorithm in Eq. (22) can be implemented in a decentralized fashion, which consists of two parts: gain and SOC deficiency. The gain becomes larger when the time to plug-off is shorter, and when the amount of cheap power is higher. The dependency on SOC deficiency ensures that vehicles with lower SOC receive higher charging power. Additionally, the dependencies show simple proportional relations. To implement this algorithm, predicted future demand from current time to the end of the valley hours, and the plug-off time of the vehicle are required. An accurate forecast of non-EV electric load is already available and used in the power transmission industry, therefore, the end of the problem horizon (end of valley hours) is readily available. The plug-off time of individual EV needs to be known, perhaps estimated from user input or learned from past behaviors. Also, we assume that the number of EVs connected to the grid can be estimated from historical data, or from the binary on–off data from their smart chargers. Therefore, the controller is implementable in a decentralized way using today's technology. The control algorithm is simple and the computation can be done locally. Information from vehicle to grid is not required—except the binary plug-in data. The only information that needs to broadcast from the grid to the vehicles is the predicted cheap power trajectory.

4. Frequency regulation

Another important attribute of EV charging is its fast response time. EV batteries have a faster power slew rate than conventional power generators such as steam turbines. Due to this characteristic, EVs can replace some of the regulation service units. Battery charging will not be deteriorated by the regulation control because regulation is a zero-energy service that compensates for minute-to-minute fluctuations [3]. Long-horizon services (>10 min) such as load following or energy balancing will continue to be provided by other power sources.

The regulation control using EV batteries is designed as a frequency droop control:

$$P_{EV,REG}(t,n) = k_f(t)(\omega(t,n) - \omega_0), \tag{24}$$

where $\omega(t, n)$ is the frequency measured by EV # n at time t. $k_f(t)$ is the droop control gain that is time varying and is broadcast by the grid operator. From the point of view of the grid, the effective

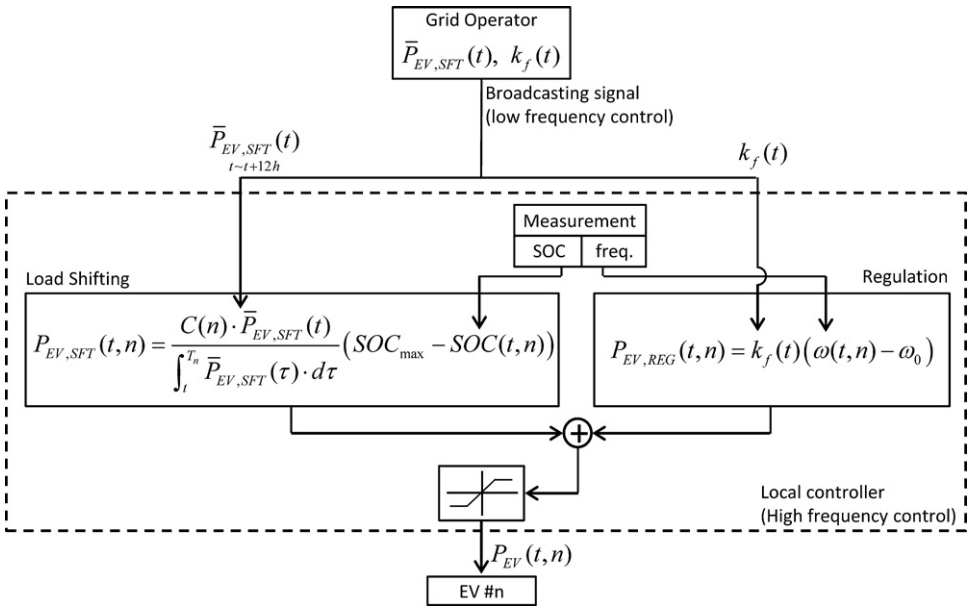

Fig. 11. The final control structure. Grid operator broadcast signals to each EV. The controller inside the dashed box is located in each EV.

gain (k_{eff}) depends on the number of EVs connected to the grid, as follows:

$$P_{REG}(t) = \sum_{n=1}^{N} P_{EV,REG}(t,n) = N_{EV}(t)k_f(t)(\omega(t,n)-\omega_0)$$
$$= k_{eff}(t)(\omega(t,n)-\omega_0). \quad (25)$$

A constant effective gain is preferable for consistent regulation performance. However, when $N_{EV}(t)$ is very small, constant effective gain cannot be achieved. Therefore, we propose the following adaptive gain:

$$k_f(t) = \frac{K_f}{N_{EV,NOM}(t)}, \quad (26)$$

where K_f is the desired overall gain and $N_{EV,NOM}(t)$ is the nominal number of vehicles that only need to be updated periodically. K_f is complementary to k_p in Eq. (2) and they determine the amount of the frequency droop. The control parameters of regulation plants, such as K_f, k_p, are usually determined from the maximum available regulation power dividend by the maximum allowable frequency droop. Mismatch between the true number of EVs and its nominal value will cause slight variation in effective regulation gain. When the total number of EVs is small, they may not provide adequate regulation capability.

5. Algorithm integration

The load shifting algorithm and the regulation algorithm were designed to achieve their individual objectives. However, in concept, the algorithms will not interfere with each other because of their time-scale separation. Therefore, the two controllers are combined in a simple way:

$$P_{EV}(t,n) = sat\{P_{EV,SFT}(t,n) + P_{EV,REG}(t,n),$$
$$-P_{EV\,\lim}(t), P_{EV\,\lim}(t),\}, \quad (27)$$

where *sat* is a saturation function that takes into account the power limit of EV batteries. The overall control structure is shown in Fig. 11. The controller in the grid operator side computes $\bar{P}_{EV,SFT}(t)$ and $k_f(t)$ to broadcast to EVs. The broadcasting is done at a very low time frequency such as every ten minutes. The controller in the EV charger computes charging power for load shifting and for regulation using local measurement signals: SOC and AC frequency. This controller performs computation at a higher rate such as every 10 s.

6. Algorithm verification

The decentralized control algorithm was verified using six simulation scenarios categorized into three groups, as summarized in Table 2. The first group was designed to verify the performance of the load shifting algorithm under perfect information. Scenario 1 uses the demand profile shown in Fig. 1. Scenario 2 uses a demand profile that has double valleys shown in Fig. 10(b). The second group was designed to verify the performance of the load shifting controller under imperfect estimation. Scenario 3 uses the single valley profile with inaccurate $N_{EV}(t)$: the estimated $N_{EV}(t)$ is assumed to be delayed by 1 h from the true values. Scenario 4 also uses the same demand profile but the total number of EVs is 50% higher than the expected (2 million vehicles were expected but 3 million vehicles were plugged in). The last group was designed to evaluate the integrated algorithm (load shifting and regulation). Scenario 5 uses the single valley demand profile with a wind power source. Scenario 6 uses the same demand profile and the wind power source but the regulation controller was turned off to investigate the effect of EV's regulation operation. In these scenarios, we assumed perfect estimation except wind power forecasting. The rest of the simulation conditions were common for every scenario as follows: the simulation horizon was 24 h; the time step was 10 s; the plug-in/off time and the initial SOCs were randomly generated but identical for each simulation; and, the number of vehicle fleets was 1000, which means that each one represented 2000 EVs (2500 EVs for Scenario 4).

6.1. Load shifting algorithm with perfect estimation

The simulation results for Scenarios 1 and 2 are plotted in Fig. 12 and the performance summary is shown in Table 3. In both

Table 2
Simulation scenarios to verify the performance of the proposed control algorithms.

Scenario	Controller	$N_{EV}(t)$ estimation	Renewable power	Demand profile
1	Load shifting	Perfect	No	Single valley
2	Load shifting	Perfect	No	Double valley
3	Load shifting	1 h delayed	No	Single valley
4	Load shifting	25% less	No	Single valley
5	Shifting + regulation	Perfect	Yes	Single valley
6	Load shifting	Perfect	Yes	Single valley

scenarios, the baseline controller allows unmitigated charging. Therefore, it achieved the best battery charging performance but the power generation cost was much higher than the controlled cases. The decentralized load shifting algorithm effectively shifted the peak load into the valley, achieving lower generation cost (5–8% reduction) without losing the battery charging performance.

6.2. Load shifting algorithm with imperfect estimation

Scenario 3 was designed to test the robustness against number of electrified vehicles, $N_{EV}(t)$. We assumed that the estimated vehicle number was a time delayed version of the actual number and the results are shown in Fig. 13(a) and (b). Even though the inaccurate estimation slightly degraded the charging performance (from 99.99% of Scenario 1 to 99.93% of Scenario 3) the valley filling worked well and the degradation was small. Scenario 4 was designed to study the effect of more EVs than expected and the results are shown in Fig. 13(c) and (d). The expected number of EVs was 2 million but the number of connected EVs was 3 million. The required charging energy was much higher than the energy available in the valley hours. As a result, the more expensive power source is used. However, battery charging still happens in an orderly manner and the charging performance was still high (99.92%), as shown in Table 3. These two simulations show that the performance of the decentralized load shifting algorithm is quite robust and vehicle charging completion took priority over other objectives. To achieve leveled valley filling in the case of 3 million EVs, the grid operator has to compute $\tilde{P}_{EV,SFT}(t)$ using larger $L_1 + L_2$ than in the case of 2 million EVs.

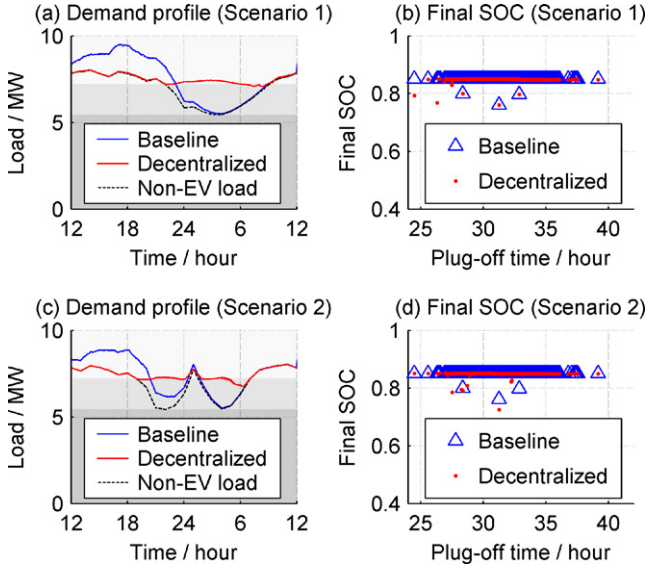

Fig. 12. Verification of the load shifting controller under perfect estimation.

6.3. Integrated controller with wind power uncertainties

Simulations with the integrated controller were performed to evaluate two important aspects: whether the load shifting performance and the final SOC are degraded by integration of the regulation controller and how the regulation controller is beneficial. Scenario 5 uses the integrated (load shifting + regulation) algorithm with the single valley demand profile and the wind power source profile shown in Fig. 3. Scenario 6 uses only the load shifting controller with the single valley demand profile and the wind power source. In both scenarios, the forecasted demand profile and forecasted wind power profile were used to determine the required power generation from the base plants. The wind power uncertainties are compensated by the regulation services from the conventional regulation plants and EVs in Scenario 5 and only by the conventional regulation plants in Scenario 6.

The results are plotted in Fig. 14 and summarized in Table 4. The load shifting performance and the charging performance of Scenario 5 were not degraded compared to those in Scenario 6, which confirms that the regulation controller does not degrade the load shifting performance and the charging performance, which is expected. Furthermore, the regulation controller improved the frequency regulation with reduced reliance on conventional regulation power plants, which indicates the possibility of cost reduction in regulation services.

In summary, as shown in Fig. 15, the decentralized charging control algorithm reduces generation cost and CO_2 emissions without degrading EV charging completion rates. In the meantime, the algorithm contributes to the frequency regulation services. The

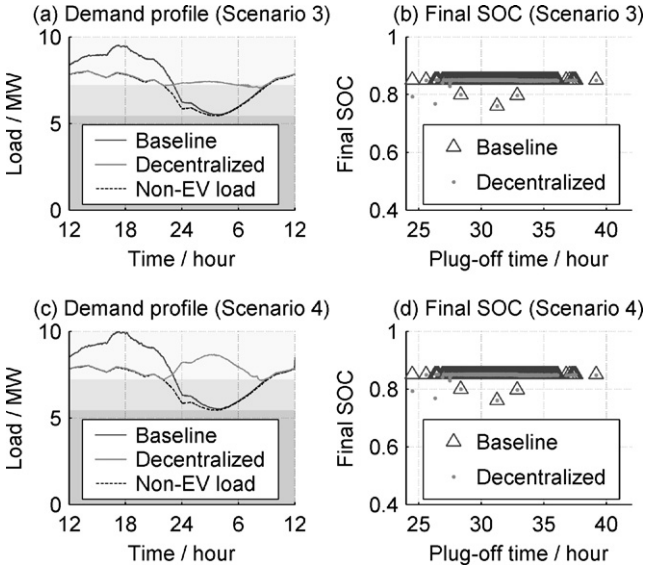

Fig. 13. Verification of the load shifting controller under imperfect: (a) when $N_{EV}(t)$ estimation is inaccurate, (b) number of total EVs are more than expected.

Table 3
Performance of the load shifting algorithm compared to the baseline and LP optimal results.

Scenario	Controller	Generation cost[a]	CO_2 emission[a]	Charging performance[b] (%)
	Baseline	1	1	100
1	LP optimal	0.907	0.969	100
	Decentralized	0.923	0.976	99.99
	Baseline	1	1	100
2	LP optimal	0.908	0.970	100
	Decentralized	0.948	0.985	99.98
3	Baseline	1	1	100
	Decentralized	0.923	0.976	99.93
4	Baseline	1	1	100
	Decentralized	0.925	0.976	99.92

[a] Generation cost and CO2 emission are normalized by the values of the baseline cases.
[b] Charging performance is the sum of all served SOCs divided by the sum of all SOCs of the baseline controller case.

Table 4
Performance of the integrated algorithm compared to the load shifting algorithm only case.

Scenario	Controller	Generation cost	Charging performance (%)	Regulation power[a] (MW)	Frequency deviation[b] (Hz)
5	Shifting + Regulation	0.918	99.98	0.116	0.069
6	Load shifting	0.917	99.98	0.146	0.087

[a] Regulation power is the root-mean-squared power output of the conventional regulation plant.
[b] Frequency deviation is the root-mean-squared frequency deviation from 60 Hz.

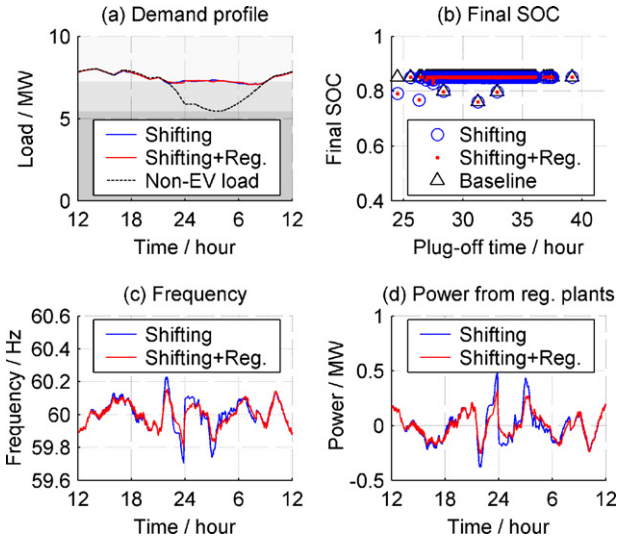

Fig. 14. Verification of the integrated algorithm: the performance of the integrated algorithm compared to the load shifting algorithm only case.

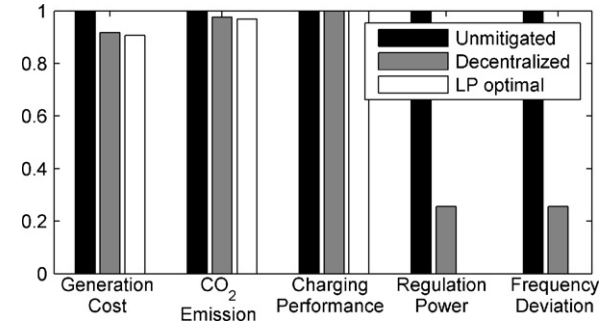

Fig. 15. Comparison of performance indices normalized by the unmitigated case (Scenario 5). The performance of frequency regulation is not applicable to the LP optimal results.

load shifting performances of decentralized controller are closed to the LP optimal performances and the frequency regulation performance is four times better than the unmitigated case while reducing regulation power by 75%.

7. Conclusions

This paper presents the design of a decentralized charging algorithm for electrified vehicles. The algorithm had two objectives: load shifting for efficiency and frequency regulation for power quality. The load shifting algorithm mimics the behavior of a global optimal solution obtained through the linear programming technique. The developed load shifting algorithm requires four pieces of information: forecasted base load profile, estimated number of plugged vehicles, estimated plug-off time, and the battery SOC of the vehicle being charged. The regulation algorithm is based on power-frequency droop. Simulation studies show that the proposed algorithm minimizes electricity generation cost and CO_2 emissions and reduces the usage of the conventional regulation power plants without compromising battery charging performance.

Acknowledgements

This work was supported by National Science Foundation EFRI-RESIN project through grant number 0835995.

Appendix.

Suppose an optimal solution exists when the conditional constraints shown in Eq. (15) are violated at t_1. Note that the following conditions hold at any time.

$$P(t_1) = q_1(t_1) + q_2(t_1) + q_3(t_1), \quad 0 \le q_1(t) \le L_1,$$
$$0 \le q_2(t) \le L_2, \quad 0 \le q_3(t), \quad 0 < c_1 < c_2 < c_3.$$

(i) $0 \le P(t_1) \le L_1$

$$\begin{aligned}
J^* &= \sum_{t=0}^{t_1-1} C(P(t)) + \sum_{t=t_1+1}^{T} C(P(t)) + c_1 q_1(t_1) + c_2 q_2(t_1) + c_3 q_3(t_1) \\
&= \sum_{t=0}^{t_1-1} C(P(t)) + \sum_{t=t_1+1}^{T} C(P(t)) + c_1 P(t_1) - c_1 P(t_1) + c_1 q_1(t_1) + c_2 q_2(t_1) + c_3 q_3(t_1) \\
&= \sum_{t=0}^{t_1-1} C(P(t)) + \sum_{t=t_1+1}^{T} C(P(t)) + c_1 P(t_1) - c_1(q_1(t_1) + q_2(t_1) + q_3(t_1)) + c_1 q_1(t_1) + c_2 q_2(t_1) + c_3 q_3(t_1) \\
&= \sum_{t=0}^{t_1-1} C(P(t)) + \sum_{t=t_1+1}^{T} C(P(t)) + c_1 P(t_1) + (c_2 - c_1) q_2(t_1) + (c_3 - c_1) q_3(t_1) \ge \sum_{t=0}^{t_1-1} C(P(t)) + \sum_{t=t_1+1}^{T} C(P(t)) + c_1 P(t_1)
\end{aligned}$$

The equality holds only when $q_2(t_1) = q_3(t_1) = 0$. Therefore, the optimal solution is achieved when $q_1(t_1) = P(t_1)$ and $q_2(t_1) = q_3(t_1) = 0$.

(ii) $L_1 \le P(t_1) \le L_1 + L_2$

$$\begin{aligned}
J^* &= \sum_{t=0}^{t_1-1} C(P(t)) + \sum_{t=t_1+1}^{T} C(P(t)) + c_1 q_1(t_1) + c_2 q_2(t_1) + c_3 q_3(t_1) \\
&= \sum_{t=0}^{t_1-1} C(P(t)) + \sum_{t=t_1+1}^{T} C(P(t)) + c_1 L_1 + c_2 L_2 + c_3(P(t_1) - L_1 - L_2) - c_1 L_1 - c_2 L_2 - c_3(P(t_1) - L_1 - L_2) + c_1 q_1(t_1) + c_2 q_2(t_1) + c_3 q_3(t_1) \\
&= \sum_{t=0}^{t_1-1} C(P(t)) + \sum_{t=t_1+1}^{T} C(P(t)) + c_1 L_1 + c_2 L_2 + c_3(P(t_1) - L_1 - L_2) + (c_3 - c_1)(L_1 - q_1(t_1)) + (c_3 - c_2)(L_2 - q_2(t_1)) \\
&\ge \sum_{t=0}^{t_1-1} C(P(t)) + \sum_{t=t_1+1}^{T} C(P(t)) + c_1 L_1 + c_2 L_2 + c_3(P(t_1) - L_1 - L_2)
\end{aligned}$$

The equality holds only when $q_1(t_1) = L_1$, $q_3(t_1) = 0$. Therefore, the optimal solution is achieved when $q_1(t_1) = L_1$, $q_2(t_1) = P(t_1) - L_1$, and $q_3(t_1) = 0$.

(iii) $P(t_1) \ge L_1 + L_2$

$$\begin{aligned}
J^* &= \sum_{t=0}^{t_1-1} C(P(t)) + \sum_{t=t_1+1}^{T} C(P(t)) + c_1 q_1(t_1) + c_2 q_2(t_1) + c_3 q_3(t_1) \\
&= \sum_{t=0}^{t_1-1} C(P(t)) + \sum_{t=t_1+1}^{T} C(P(t)) + c_1 L_1 + c_2 L_2 + c_3(P(t_1) - L_1 - L_2) - c_1 L_1 - c_2 L_2 - c_3(P(t_1) - L_1 - L_2) + c_1 q_1(t_1) + c_2 q_2(t_1) + c_3 q_3(t_1) \\
&= \sum_{t=0}^{t_1-1} C(P(t)) + \sum_{t=t_1+1}^{T} C(P(t)) + c_1 L_1 + c_2 L_2 + c_3(P(t_1) - L_1 - L_2) + (c_3 - c_1)(L_1 - q_1(t_1)) + (c_3 - c_2)(L_2 - q_2(t_1)) \ge \sum_{t=0}^{t_1-1} C(P(t)) + \sum_{t=t_1+1}^{T} C(P(t)) + c_1 L_1 + c_2 L_2 + c_3(P(t_1) - L_1 - L_2)
\end{aligned}$$

The equality holds only when $q_1(t_1) = L_1$, $q_2(t_1) = L_2$. Therefore, the optimal solution is achieved when $q_1(t_1) = L_1$, $q_2(t_1) = L_2$, and $q_3(t_1) = P(t_1) - L_1 - L_2$.

The results of (i)–(iii) contradict the assumption, which implies that the conditional constraints are satisfied when the optimal solution exists, in other words, the constraints are not active.

References

[1] M. Kintner-Meyer, K. Schneider, R. Pratt, Electric Utilities Environmental Conference, Tucson, AZ, 2007.
[2] W. Kempton, Transportation Research. Part E, Logistics and Transportation Review 2 (1997) 157.
[3] B.J. Kirby, Frequency regulation basics and trends, Oak Ridge National Laboratory, Oak Ridge, Tennessee, 2004.
[4] W. Kempton, J. Tomic, Journal of Power Sources 144 (2005) 268–279.
[5] W. Kempton, J. Tomic, Journal of Power Sources 144 (2005) 280–294.
[6] J.A. Peças Lopes, S.A. Polenz, C.L. Moreira, R. Cherkaoui, Electric Power Systems Research 80 (2010) 898–906.
[7] E. Sortomme, M.A. El-Sharkawi, IEEE Transactions on Smart Grid 2 (2011) 131–138.
[8] Y. Ota, H. Taniguchi, T. Nakajima, K.M. Liyanage, A. Yokoyama, International Conference on Industrial and Information Systems 2009, 2009, pp. 414–418.
[9] S. Han, S. Han, K. Sezaki, IEEE Transactions on Smart Grid 1 (2010) 65–72.
[10] D. Lemoine, D.M. Kammen, A.E. Farrell, Environmental Research Letters 3 (2008) 014003.
[11] P. Denholm, W. Short, An evaluation of utility system impacts and benefits of optimally dispatched plug-in hybrid electric vehicles, National Renewable Energy Laboratory (NREL), Golden, CO, 2006.
[12] J. Tomic, W. Kempton, Journal of Power Sources 168 (2007) 459–468.
[13] Z. Ma, D. Callaway, I. Hiskens, 49th IEEE Conference on Decision and Control (CDC), 2010, pp. 206–212.
[14] D.S. Callaway, I.A. Hiskens, Proceedings of the IEEE 99 (2011) 184–199.
[15] S.H. Lee, C.L. Wilkins, IEEE Transactions on Power Apparatus and Systems PAS-102 (1983) 1007–1013.

[16] J.C. Laurent, G. Desaulniers, R.P. Malhame, F. Soumis, IEEE Transactions on Power Systems 10 (1995) 1389–1400.
[17] D.-C. Wei, N. Chen, IEEE Transactions on Power Systems 10 (1995) 307–313.
[18] FERC, Annual Electric Control and Planning Area Report, 2008. http://www.ferc.gov/docs-filing/forms.asp#714.
[19] P. Kundur, N.J. Balu, M.G. Lauby, Power System Stability and Control, McGraw-Hill, New York, 1994, pp. 128–136.
[20] N. Buddhangkuranont, Analysis of Interstate Highway 5 Hourly Traffic Via Functional Linear Models, Master, Statistics, Los Angeles, 2009.
[21] NREL, Eastern Wind Dataset. http://www.nrel.gov/wind/integrationdatasets/eastern/methodology.html.
[22] G. Masters, Renewable and Efficient Electric Power Systems, John Wiley & Sons, New Jersey, 2004.
[23] Department of Energy, Carbon Dioxide Emissions from the Generation of Electric Power in the United States, Department of Energy, Washington, DC, 2000.
[24] World Nuclear Association, Greenhouse Gas Emissions from Power Generation. http://www.world-nuclear.org/why/default.aspx?id=17574&terms=co2%20emissions.
[25] E.S. Rubin, A.B. Rao, C. Chen, GHGT-7, Vancouver, Canada, 2004.
[26] A. Mackay, Journal of Environmental Quality 37 (2008) 2407.